Hindawi
Geofluids
Volume 2022, Article ID 5686814, 12 pages
https://doi.org/10.1155/2022/5686814

Research Article

Superimposed Stress Calculation of Soil Underlying Anchor Beam considering Anisotropy and Strength Nonhomogeneity

Fei Xu,[1,2] **Zhongshun Wang**,[1] **Liming Zhou**,[1] **Hemin Zheng**,[3] **Bo Liu**,[4] **Yuqiu Jiang**,[1] **and Daili Wang**[1]

[1]*Key Laboratory of Large Structure Health Monitoring and Control, Shijiazhuang Tiedao University, Shijiazhuang 050043, China*
[2]*School of Civil Engineering, Southwest Jiaotong University, Chengdu 610031, China*
[3]*China Railway Design Group Co., Ltd., Tianjin 300308, China*
[4]*School of Civil Engineering, Beijing Jiaotong University, Beijing 100044, China*

Correspondence should be addressed to Liming Zhou; ming@stdu.edu.cn

Received 6 April 2022; Revised 29 June 2022; Accepted 22 August 2022; Published 10 September 2022

Academic Editor: Yang Yu

Prestress anchor beams are an important reinforcement method for underground engineering and rock slopes, and they are crucial for maintaining the stability of civil engineering structures. In this study, the computational formula of superimposed stress of soil underlying an anchor beam was proposed in this paper, based on the assumption that the anchor beam is completely rigid and the prestress of the anchor cable is acting on soil in the form of a strip uniform load. By considering the anisotropy and strength nonhomogeneity of the saturated soft clay, the failure envelopes of the soil and the maximum effective depth underlying the anchor beam were obtained by the D-P yield criterion suitable for soft clay analysis. Furthermore, the experimental comparisons with the previous findings were used to validate the proposed approach. The proposed method was valid to assess the maximum effective depth. Considering the influence of the factors on the failure envelopes of soil, a parametric study was carried out to optimize the design of the prestressed anchor cable. The findings of this study provide a theoretical basis for designing prestressed anchor cables; these can also be used to predict the response of prestressed anchor cables as well as to optimize the design of the cables, such as the anchorage length of cable and grouting radius.

1. Introduction

Slope stability is a crucial issue in the field of geotechnical engineering; it is principally influenced by the properties of geological discontinuities of slope, and various approaches have been proposed for the slope stability analysis [1–4]. Du et al. [1] proposed a new method to evaluate slope stability in large open-pit mines based on a comprehensive investigation of the geometry and shear strength of the geological discontinuities; the results were in good agreement with field observation. Tang et al. [2] proposed a formula for calculating the safety factor of rock slope considering the effect of locked sections. Yuan et al. [3] studied the laws of slope displacement and the changing positions of a sliding surface during the filling process by using the finite element software PLAXIS. Chen et al. [4] proposed a new modified strength reduction method to calculate the decay law of slope strength by applying the respective reduction factors in a strength reduction technique. In recent decades, anchors have become one of the popular methods for slope reinforcement; in particular, prestressed anchor cables have been extensively applied in geotechnical engineering. By installing prestressed anchor cables, the self-bearing capacity of rock and soil can be fully mobilized, and the forces acting on the supporting structure can be optimized [5]. Therefore, "anchor cable rigid beam" systems are becoming popular; prestressed anchor cables are also essential for reinforcement projects such as high slopes and deep foundation pits, as presented in Figure 1.

In the past several decades, many studies have analyzed the behaviors of prestressed anchor cables by using various methods such as theoretical analyses [6–8], model tests

(a) (b)

Figure 1: Application of prestressed anchor cable: (a) used in a high slope and (b) used in a deep foundation pit.

[9–11], and numerical simulations [12–16]. Wang et al. [9] conducted pull-out tests for anchor cables for revealing the failure mechanisms and the constitutive relation; for anchorage segments, the failure mechanism displayed the pulling failure at first, followed by pulling and shearing failures. Yang et al. [12] studied the variation of tension in prestressed anchor cables based on field monitoring; they summarized the variation features of anchor tension considering the install positions on a single anchor pile, anchoring strata, and locations on the plane of the foundation pit. Wu et al. [17] conducted shaking table tests to investigate the seismic response of a slope reinforced by prestressed anchor cables and double-row antisliding piles, and they revealed that the reinforced slope had good overall stability. Sun et al. [18] proposed a large deformation anchor cable support system and used 3DEC software and a series of field tests to study the effect of applying an NPR anchor cable support system, showing that the NPR anchor cable support system achieved good results in tunnel engineering. Yuan et al. [19] established a similar method to simulate anchors in the combined structure and derived the inherent internal force and algorithmic tangent stiffness of the anchor model, revealing that the nonlinearity of the anchor was mainly caused by the interface failure and anchor yielding. Contemporary studies have mainly focused on a homogeneous and isotropic homogeneity stratum without considering the effect of load dispersion induced by the anchor beam. Few studies have calculated superimposed stress and the plastic failure zone of soil underlying the anchor beam, especially in terms of the saturated soft clay considering the anisotropy and strength nonhomogeneity.

Saturated soft clay has high permeability, large deformation, high compressibility, anisotropy, and strength nonhomogeneity. Thus, soil cohesive force considerably influences the direction of the maximum principal stress, and it varies at different soil depths [20, 21] (described in detail in Section 3.1).

In this study, the anchor beam is assumed to be completely rigid, a prestressed anchor cable is applied to soil in the form of uniform load, and the computational formula of the superimposed stress of soil underlying the anchor beam is proposed. Considering the anisotropy and strength nonhomogeneity of saturated soft clay, the plastic failure envelopes of soil and the maximum effective depth underlying the anchor beam are obtained using the D-P yield criterion. To evaluate the validity of the proposed method, the results of the maximum effective depth are compared with those presented in previous studies. Good agreement is observed between the results of this study and those of previous studies, which indicates the validity of the proposed method. Finally, to optimize the design of the prestressed anchor cable, a parametric study is conducted by analyzing the influence of anisotropy on the plastic failure envelopes.

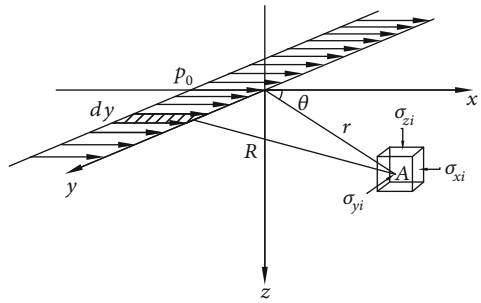

Figure 2: Superimposed stress of soil underlying the anchor beam induced by a horizontal line load.

2. Superimposed Stress of Soil Underlying the Anchor Beam

As described by Huang [22] and He [23], the distribution of foundation stress derived from the elastic theory is in line with that obtained from the finite element method, demonstrating that the influence of the distribution of foundation stress induced by the nonlinearity, layered distribution, and plastic deformation of soil can be considered negligible. Therefore, in this study, it is assumed that the superimposed stress of soil underlying an anchor beam can be calculated using the elastic theory. It is assumed that the anchor beam is perfectly rigid, and the prestress of the anchor cable acting on the rigid beam is considered equivalent to a uniformly

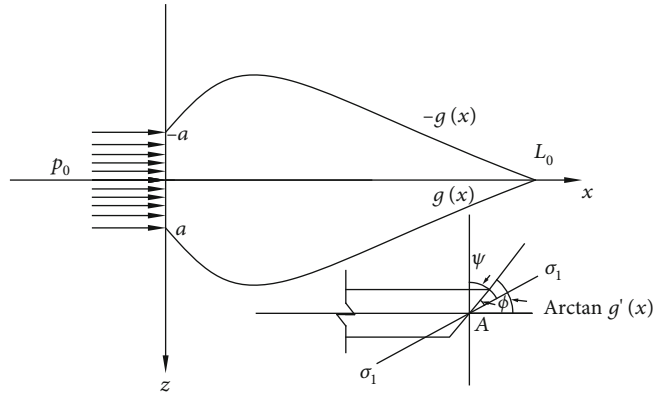

Figure 3: Calculation model of failure envelopes of soil underlying the anchor beam by horizontal line load.

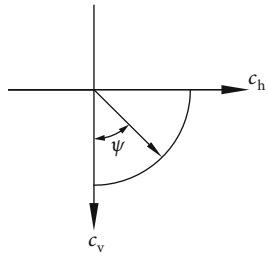

Figure 4: Anisotropy of soil.

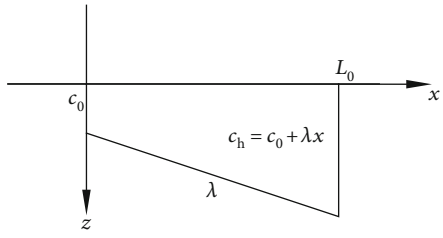

Figure 5: Nonhomogeneity of soil.

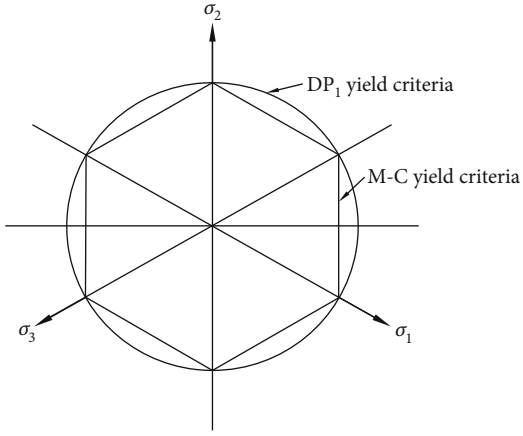

Figure 6: Yield curves of M-C and DP1 yield criteria in the π plane.

distributed strip load. The simplified calculation model of the load acting on the beam is shown in Figure 2.

Using the method of Melan integration [24], when the horizontal line load p_0 is applied to soil through the origin of coordinate (Figure 2), the superimposed stress acting at an arbitrary point A of soil underlying the anchor beam can be obtained using

$$\sigma_{xi} = \frac{2p_0x^3}{\pi[x^2 + g^2(x)]^2}, \tag{1}$$

$$\sigma_{zi} = \frac{2p_0xg^2(x)}{\pi[x^2 + g^2(x)]^2}, \tag{2}$$

$$\tau_{(xz)i} = \frac{2p_0x^2g(x)}{\pi[x^2 + g^2(x)]^2}, \tag{3}$$

$$\tau_{(xy)i} = 0, \tag{4}$$

$$\tau_{(zy)i} = 0. \tag{5}$$

Based on the general Hooke's law and plane strain assumption, the shear strain, ε_{yi}, can be expressed as

$$\varepsilon_{yi} = 0. \tag{6}$$

According to Equations (1)–(6), the normal stress along the Y-axis, σ_{yi}, can be calculated using

$$\sigma_{yi} = \mu(\sigma_{zi} + \sigma_{xi}) = \mu\left[\frac{2p_0g^2(x)}{\pi[x^2 + g^2(x)]^2} + \frac{2p_0x^3}{\pi[x^2 + g^2(x)]^2}\right] = \frac{2p_0x\mu}{\pi[x^2 + g^2(x)]}, \tag{7}$$

where σ_{xi} and σ_{zi} are the normal stress along the directions of X - and Z-axes, respectively; τ_{xy}, τ_{yz}, and τ_{zx} are the shear stress on the XY, YZ, and ZX surfaces, respectively; p_0 is the horizontal line load; $g(x)$ is the function of the failure envelopes of soil; and μ is Poisson's ratio.

The width of the anchor beam is assumed to be equal to $2a$ (see Figure 3). Integrating Equations (1)~(6) along the direction of the anchor beam width, the values of σ_x, σ_z, σ_x, τ_{xz}, τ_{xy}, and τ_{zy} can be computed as given in

$$\sigma_x = \sum_{i=1}^{n}\sigma_{xi} = \int_{-a}^{a}\frac{2p_0x^3}{\pi\left\{x^2 + [g(x) - h]^2\right\}^2}dh, \tag{8}$$

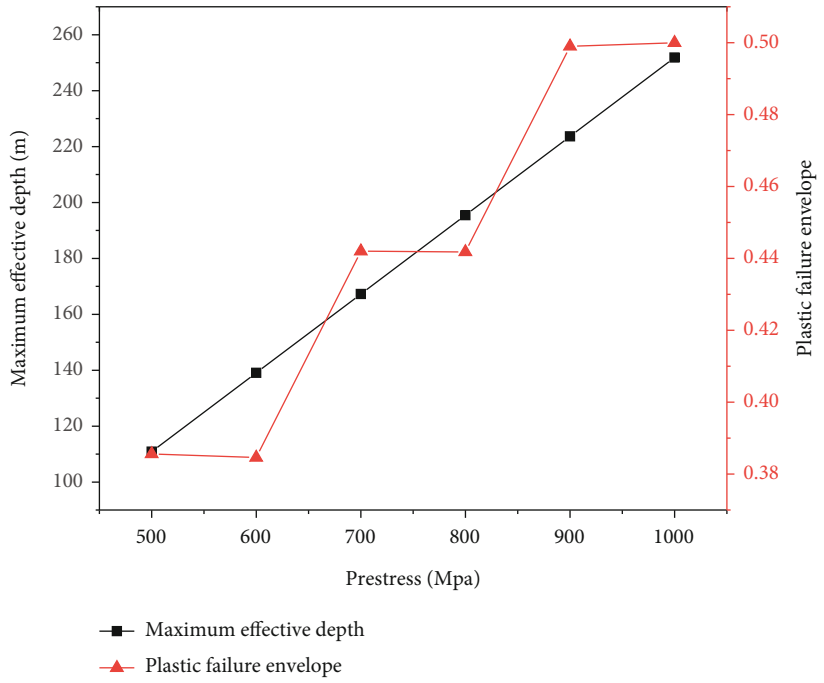

Figure 7: Failure envelopes of soil under different prestress p_0 values.

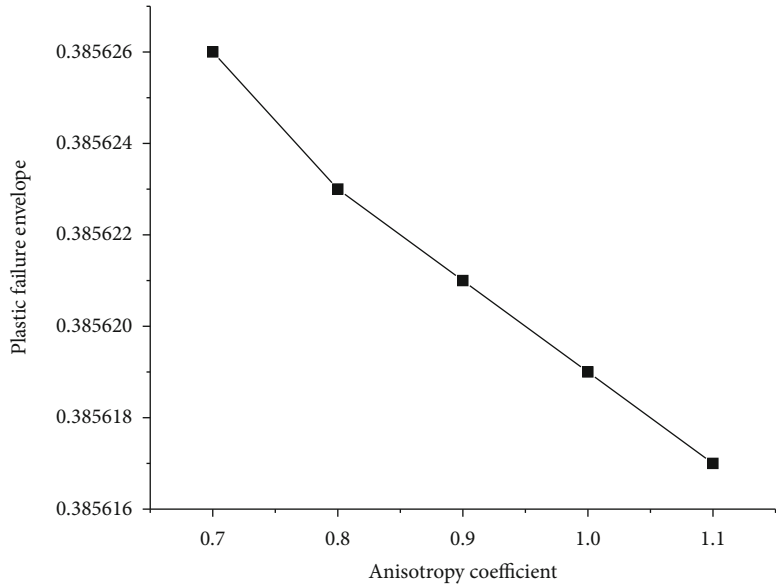

Figure 8: Failure envelopes of soil under different anisotropy coefficients ρ.

$$\sigma_z = \sum_{i=1}^{n} \sigma_{zi} = \int_{-a}^{a} \frac{2p_0 x[g(x)-h]^2}{\pi\left\{x^2+[g(x)-h]^2\right\}^2} dh, \tag{9}$$

$$\sigma_y = \sum_{i=1}^{n} \sigma_{yi} = \int_{-a}^{a} \frac{2p_0 x\mu}{\pi\left\{x^2+[g(x)-h]^2\right\}^2} dh, \tag{10}$$

$$\tau_{xz} = \sum_{i=1}^{n} \tau_{(xz)i} = \int_{-a}^{a} \frac{2p_0 x^2[g(x)-h]}{\pi\left\{x^2+[g(x)-h]^2\right\}^2} dh, \tag{11}$$

$$\tau_{xy} = 0, \tag{12}$$

$$\tau_{yz} = 0. \tag{13}$$

3. Failure Envelopes of Soil and the Maximum Effective Depth Underlying the Anchor Beam

3.1. Anisotropy and Strength Nonhomogeneity of Soil. The angle of internal friction, φ, and the cohesive force, c, can be used to predict soil strength. For nonhomogeneous and anisotropic soil, following the suggestion of [25], φ is assumed to be constant, and c is assumed to be nonhomogeneous and anisotropic [26]. As described in [27], the value of φ can be assumed to be 35°.

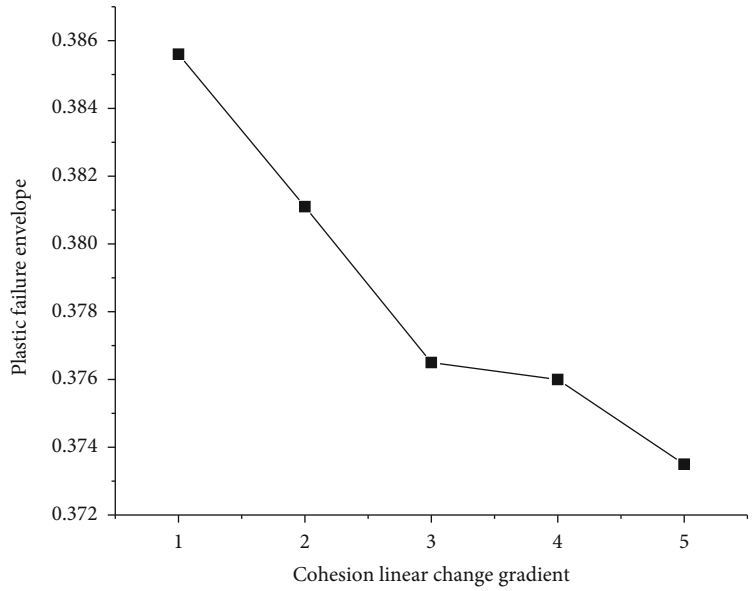

Figure 9: Failure envelopes of soil under different nonhomogeneity parameters λ.

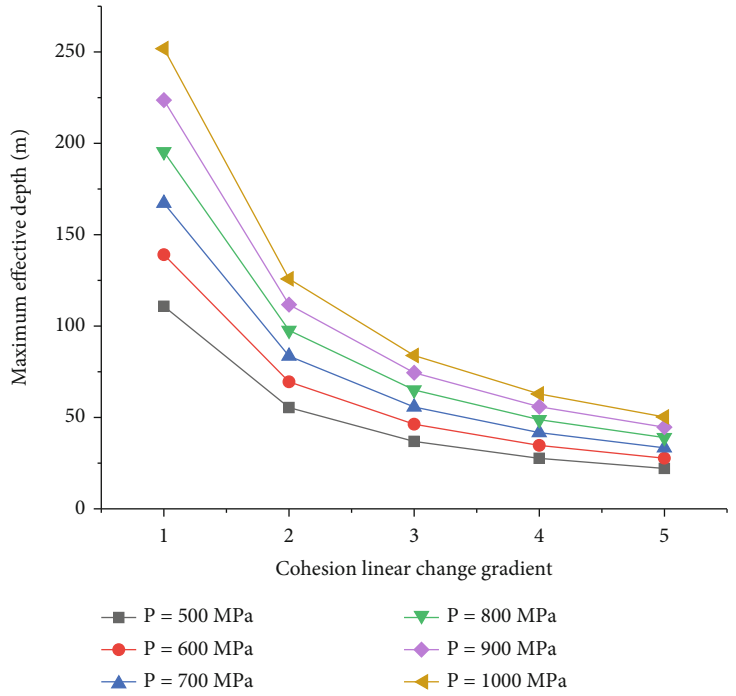

Figure 10: Maximum effective depth of soil under different nonhomogeneity parameters λ.

According to Casagrande and Carillo [28], for anisotropic clay soil, the cohesive force of saturated and undrained clay soil, c_ψ, can be obtained using

$$c_\psi = c_h + (c_v - c_h)\cos^2\psi, \tag{14}$$

$$\psi = \frac{\pi}{2} - \arctan g'(x) + \phi, \tag{15}$$

where c_h and c_v are the cohesive forces along the X- and Y-axes, respectively (Figure 4).

The coefficient of anisotropy, ρ, can be expressed as

$$\rho = \frac{c_h}{c_v}, \tag{16}$$

where the value of ρ is in the range 0.50–1.33. When the value of ρ is 1.00, soil can be assumed to be isotropic [26].

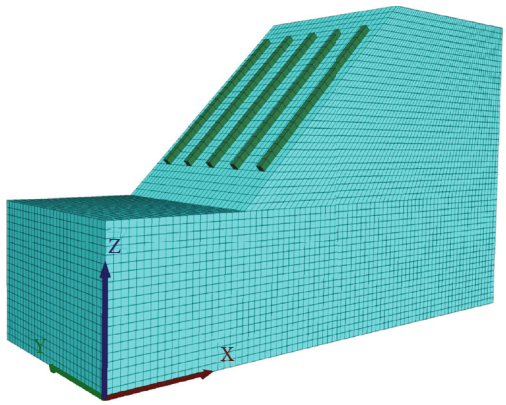

Figure 11: Numerical model sketch.

Substituting Equation (16) into Equation (14), we obtain

$$c_\psi = c_h\left(1 + \frac{1-\rho}{\rho}\cos^2\psi\right). \tag{17}$$

For saturated and undrained clay soil, the strength varies linearly with increase in depth [29–31]. As shown in Figure 5, the cohesive force in the horizontal direction c_h can be expressed using

$$c_h = c_0 + \lambda x, \tag{18}$$

where λ is the gradient of linear variation of the cohesive force and x is the value of depth along the axis direction of the cable.

Substituting Equations (17) and (18) into Equation (14), we obtain

$$c_\psi = (c_0 + \lambda x)\left(1 + \frac{1-\rho}{\rho}\cos^2\psi\right). \tag{19}$$

3.2. Failure Envelopes of Soil. The Drucker-Prager yield criterion, which is typically used as the modified model of the Mohr–Coulomb yield criterion, and a nonassociative flow rule were used herein [32]. This linear perfectly elastic–plastic yield criterion can be used to capture the shear-compression failure of soft clay with a small friction angle. In this study, the DP1 yield criterion [33] is used (Figure 6), and the yield function can be expressed as

$$F(\sigma) = f(I_1, J_2) = \alpha I_1 + \sqrt{J_2} - \kappa = 0, \tag{20}$$

$$I_1 = \sigma_x + \sigma_y + \sigma_z, \tag{21}$$

$$J_2 = \frac{1}{6}\left[(\sigma_x - \sigma_y)^2 + (\sigma_y - \sigma_z)^2 + (\sigma_z - \sigma_x)^2 + 6\left(\tau_{xy}^2 + \tau_{yz}^2 + \tau_{zx}^2\right)\right], \tag{22}$$

$$\alpha = \frac{2\sin\varphi}{\sqrt{3}\left(3 - \sin^2\varphi\right)}, \tag{23}$$

$$\kappa = \frac{6c_\psi\cos\varphi}{\sqrt{3}\left(3 - \sin^2\varphi\right)}. \tag{24}$$

Substituting Equations (8)–(13) into Equations (21) and (22), we obtain

$$I_1 = (1+\mu)\int_{-a}^{a}\frac{2p_0 x}{\pi\left\{x^2 + [g(x)-h]^2\right\}^2}dh, \tag{25}$$

$$J_2 = \int_{-a}^{a}\frac{4p_0^2x^2}{3\pi^2\left\{x^2 + [g(x)-h]^2\right\}^4}\left\{x^4\left(1-\mu+\mu^2\right) + [g(x)-h]^4 \cdot \left(1+\mu^2\right) + 2x^2[g(x)-h]^2\right\}dh, \tag{26}$$

where I_1 is the first invariant of the stress tensor and J_2 is the second principal invariant of the stress deviator tensor.

Substituting Equations (23)–(26) into Equation (20), we obtain

$$\frac{3\text{-}\sin^2\varphi}{2\sin\varphi}\sqrt{\int_{-a}^{a}\frac{x^2\left\{x^4(1-\mu+\mu^2) + [g(x)-h]^4(1+\mu^2) + 2x^2[g(x)-h]^2\right\}dh}{\left\{x^2 + [g(x)-h^2]\right\}^2}} + (1+\mu)\int_{-a}^{a}\frac{x\mathrm{d}h}{\left\{x^2 + [g(x)-h]^2\right\}^2} = \frac{3c_\psi\pi}{2p_0\tan\varphi}. \tag{27}$$

3.3. Maximum Effective Depth. Considering the symmetry, when the value of z presented in $g(x)$ is 0, the maximum effective depth along the axial direction of cable L_0 can be obtained using Equation (34).

When the value of z is 0, the boundary conditions can be expressed as follows:

$$z = g(x) = g'(x) = 0, \tag{28}$$

$$\cos\psi = 0\ (\psi = 90^\circ). \tag{29}$$

Then, we obtain

$$\sigma_{x0} = \frac{2p_0x^3}{\pi}\int_{-a}^{a}\frac{1}{\left(x^2+h^2\right)^2}dh = \frac{2p_0}{\pi}\left(\arctan\frac{a}{x} + \frac{xa}{x^2+a^2}\right), \tag{30}$$

$$\sigma_{z0} = \frac{2p_0}{\pi}\int_{-a}^{a}\frac{xh^2}{\left(x^2+h^2\right)^2}dh = \frac{2p_0}{\pi}\left(\arctan\frac{a}{x} - \frac{xa}{x^2+a^2}\right), \tag{31}$$

$$\sigma_{y0} = \mu(\sigma_{x0} + \sigma_{z0}) = \frac{4p_0\mu}{\pi}\arctan\frac{a}{x}, \tag{32}$$

$$\tau_{(xz)0} = \tau_{(zy)0} = \tau_{(yx)0} = 0. \tag{33}$$

Table 1: Material properties of the model.

Material	Density ρ (kg/m^3)	Young's modulus E (MPa)	Poisson's ratio λ	Cohesion c (kPa)	Friction ϕ (°)
Soft clay	2000	50	0.15	30	20
Anchor beam	2500	25000	0.2	3000	50

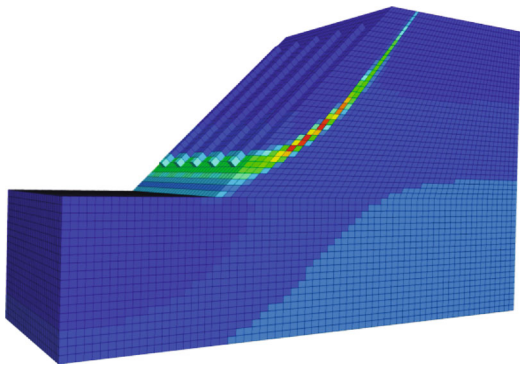

Figure 12: Initial equilibrium state of the slope.

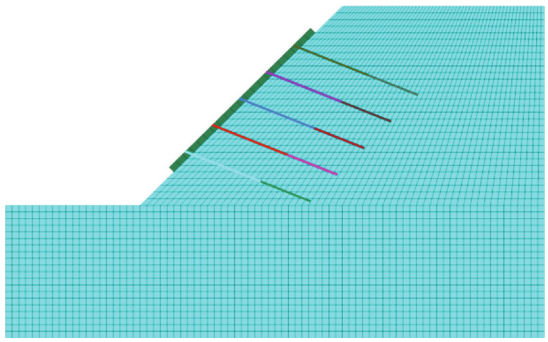

Figure 13: Slope model with cables.

Substituting Equations (30)–(33) into Equation (20), we obtain

$$\frac{3-\sin^2\varphi}{4\sin\varphi}\sqrt{(1-2\mu)^2\arctan^2\frac{a}{x}+\frac{3x^2a^2}{(x+a)^2}}+(1+\mu)\arctan\frac{a}{x}=\frac{3c_h\pi}{4p_0\tan\varphi}. \tag{34}$$

The maximum effective depth, L_0, can then be computed using Equation (34).

4. Parametric Study

To analyze the influence of parameters considered in the proposed method on the plastic failure envelopes of soil and the maximum effective depth underlying the anchor beam, a further parametric study was conducted. The value of beam width, $2a$, was adopted as 1 m; the value of Poisson's ratio, μ, of saturated soft clay was considered as 0.5; the value of initial horizontal cohesive strength, c_0, was assumed to be 30 kPa; and the value of the angle of internal friction φ was set to 20°. Considering the complexity of Equations (27) and (34), mathematical software Mathematica and Fortran 95 were used to compute the results.

4.1. Influence of Prestress on the Failure Envelopes. In this experiment, λ was set to 1, ρ was set to 1, and cable prestress, p_0, was considered to be in the range 500–1000 kPa, with increment steps of 100 kPa. Figure 7 shows that the failure envelopes of soil increase with increase in the value of prestress, p_0. The variation law of the maximum effective depth also follows the same trend.

4.2. Influence of Anisotropy on the Failure Envelopes. To analyze the influence of anisotropy on the plastic failure envelopes, λ was set to 1, and the cable prestress, p_0, was set to 500 kPa. Figure 8 shows that the failure envelopes of soil only slightly influence ρ, increasing it from 0.7 to 1.1. Thus, the shear strength of soil decreased with increase in the value of ρ, and there were small increments in the failure envelopes of soil.

4.3. Influence of Nonhomogeneity on the Failure Envelopes. To analyze the influence of nonhomogeneity on the failure envelopes, ρ was set to 1, and the prestress, p_0, of the cable was set to 500 kPa. Figure 9 shows that the plastic failure envelopes of soil decreased as λ increased from 1 to 5, with increments of 1. Thus, the shear strength of soil increased with increase in λ.

The value of ρ was set to 1, and the value of cable prestress, p_0, was in the range 500–1000 kPa, with increments of 100 kPa. Figure 10 shows that the maximum effective depth of soil underlying the anchor beam increased with increase in the value of p_0 and decreased when λ increased from 1 to 5, with increments of 1. The influence of the coefficient of anisotropy, ρ, on the failure envelopes and the maximum effective depth of soil subjected to higher stress was larger than that under the influence of lower stress.

In general, based on the clarification of the influence of parameters p_0, ρ, and λ on the plastic failure envelopes and the maximum effective depth of soil, a simple method can be provided to predict the response of the prestressed anchor cable and to optimize cable design parameters, such as the anchorage length of cable and grouting radius.

5. Verification through Numerical Simulation

To verify the critical parameters of the equations presented in Section 3, a simple model of slope and cable was built using Flac3d software. The slope was analyzed by considering the cable prestress, p_0, the coefficient of anisotropy, ρ, and the linear gradient of cohesive force, λ.

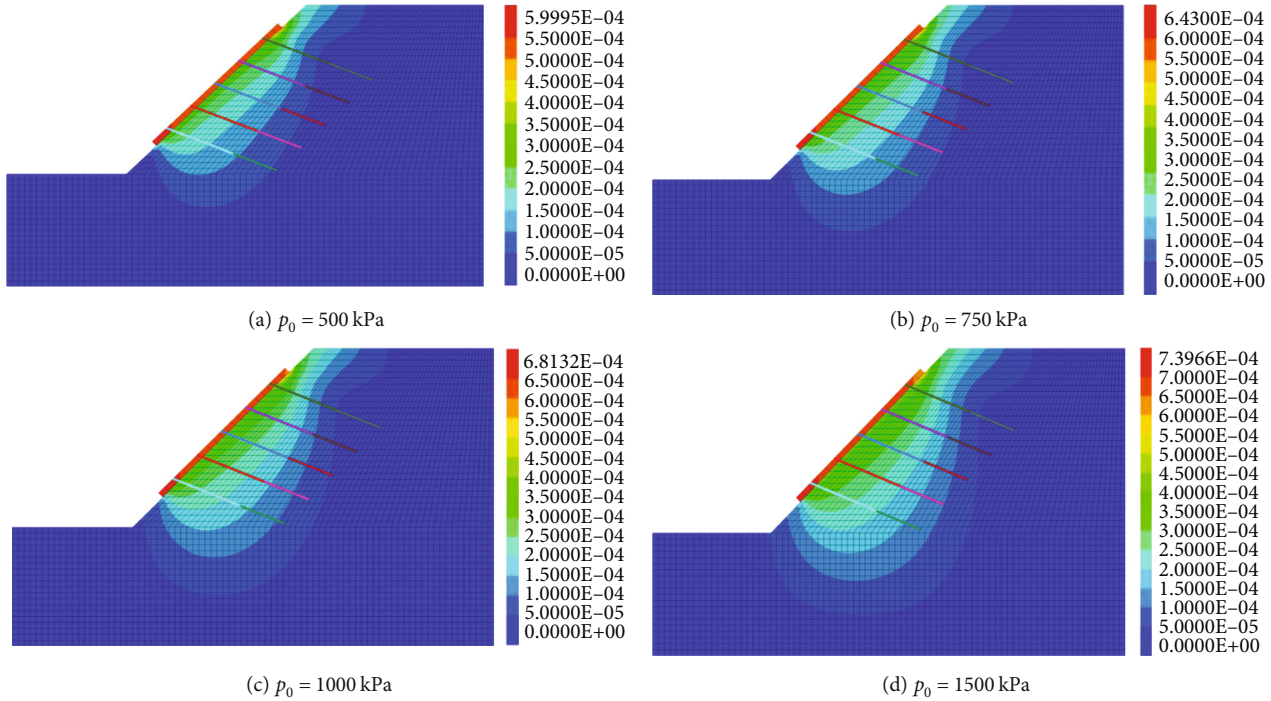

Figure 14: The displacement nephogram of the slope under different prestresses.

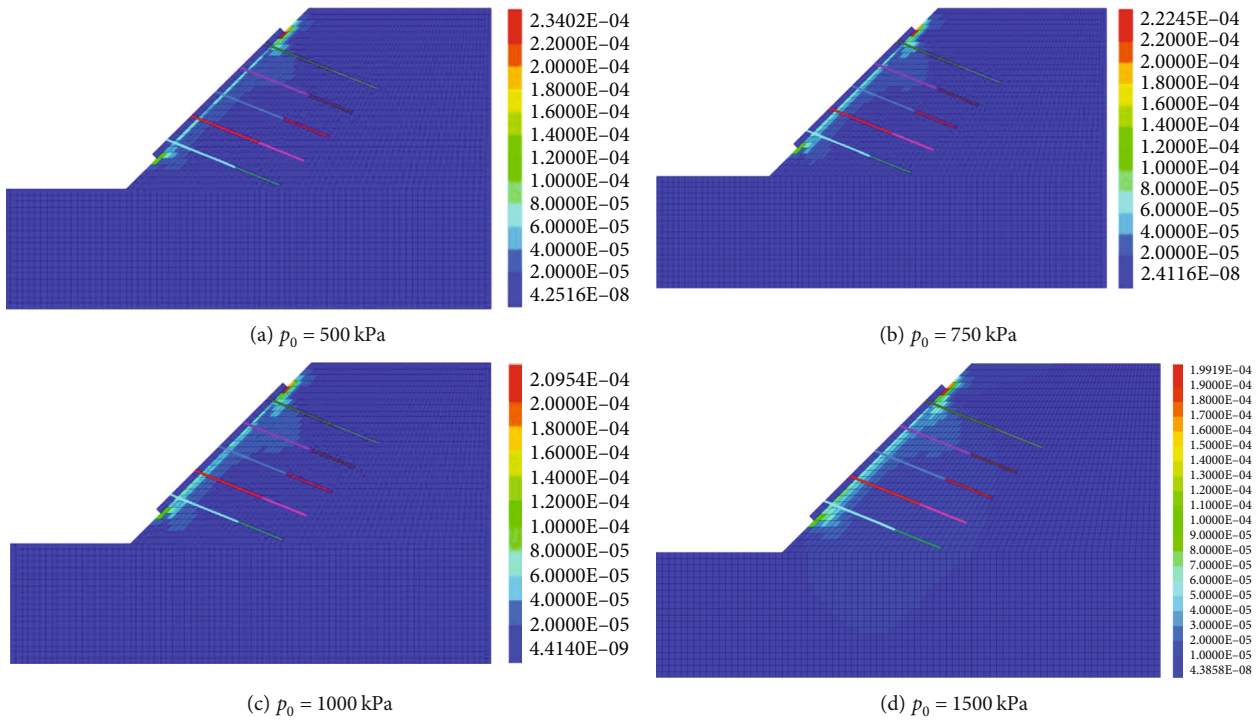

Figure 15: Maximum shear strain.

5.1. Modeling and Loading Cases. The brick element was used to simulate the slope, and the cable element was used to simulate the anchor beams. The dimensions of the slope model were length = 80 m, width = 30 m, and height = 50 m; the toe of the slope was 30 m high. Five anchor beams were set on the slope surface with dimensions of 26 m × 1 m × 1 m . The function of the beam was to distribute the prestress evenly on the slope. The bottom of the slope was fully restrained, and normal restraint was applied at the four vertical surfaces. The slope model is illustrated in Figure 11.

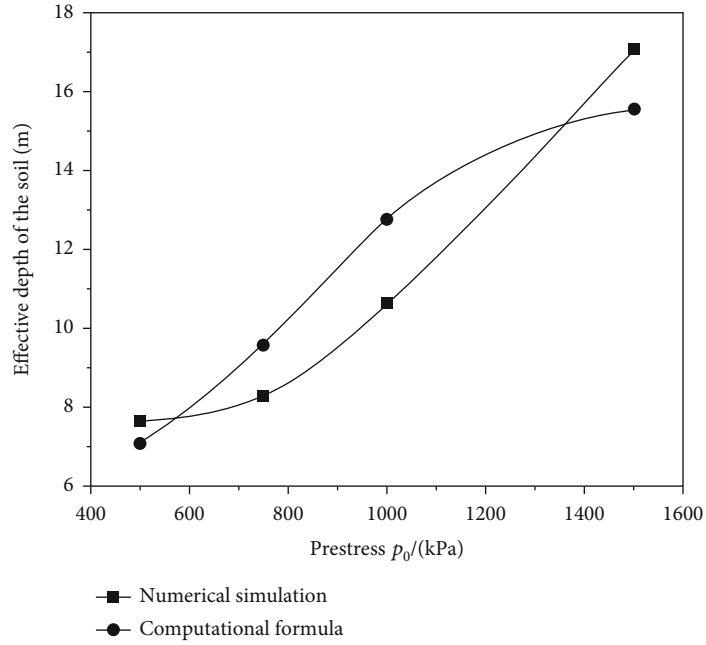

Figure 16: Maximum effective depth underlying the anchor beam.

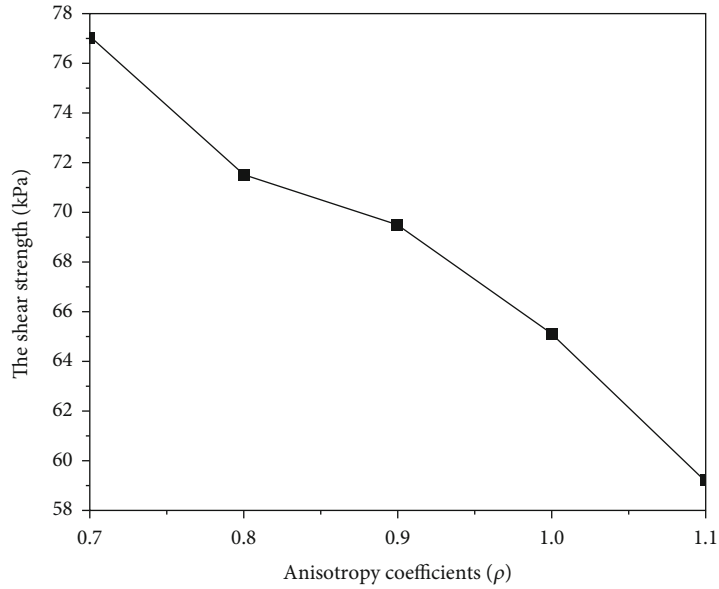

Figure 17: The variation in shear strength of soil with different anisotropy coefficients.

For soil of the slope, the Drucker-Prager ideal elastic–plastic stress-strain model was adopted, along with the Mohr–Coulomb constitutive model for anchor beams. Combined with the values suggested in Code and practical engineering, the properties of slope and beams were identified (listed in Table 1).

To ensure agreement between the behavior of the calculation model and real-time projects, an initial ground stress equilibrium is necessary. The factor of safety of the slope was 1.28, indicating sufficient stability. The initial state is shown in Figure 12. After the first equilibrium, elements such as prestress cables and the interface between beams and slope were built. The cables were set through the beams using the built-in structural element (length = 20 m, interval = 4 m, and inclination angle = 22°) of Flac3d software. The prestress cable comprised a free section (length = 12 m) and an anchorage section (length = 8 m). The anchorage part was divided into eight parts for high calculation accuracy. Young's modulus of the cable was 200 GPa, the cross-sectional area was 0.00176 m^2, grout perimeter was 0.15 m, grout cohesion was 5.0×10^6 N/m, grout stiffness was 1.0×10^7 N/m^2, grout friction was 33°,

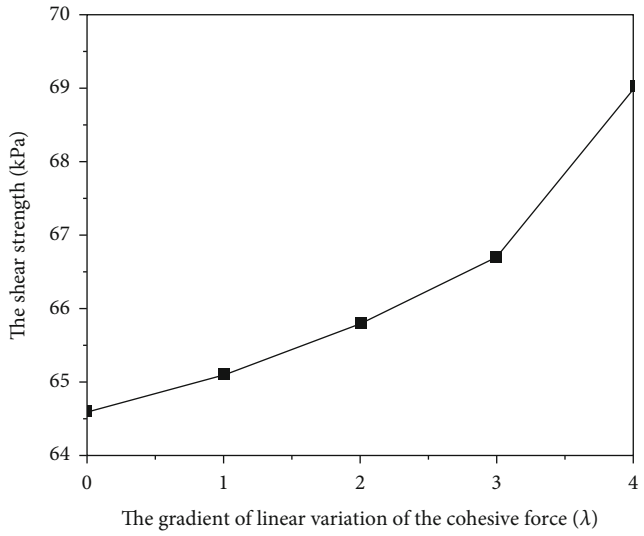

Figure 18: Variation in shear strength with the cohesion gradient.

and yield tension was 1×10^5 kN; the slope model with cables is shown in Figure 13.

To verify the theoretical formulas, the prestress of cables, p_0, the anisotropy coefficient of saturated soft clay, ρ, and the linear gradient of cohesive force, λ, were considered successively to obtain the failure response of the prestressed cables. Thus, three cases were carried out in the numerical simulation, presented below.

Case 1. ρ was set to 1, and λ was set to 0. p_0 was set to 500 kPa, 750 kPa, 1000 kPa, and 1500 kPa.

Case 2. λ was set to 0, and p_0 was set to 500 kPa. ρ was increased from 0.7 to 1.1, with increments of 0.1.

Case 3. ρ was set to 1, and p_0 was set to 500 kPa. The value of λ was increased from 0 to 4, with increments of 1.

5.2. Calculation Results. For the three cases, the critical parameters were specifically concerned, and the failure responses of the cables were obtained, which were comparable with the theoretical formulas.

In Case 1, the shear strain indicated the slide state of the slope, and the maximum effective depth of soil underlying the anchor beam was obtained. Figure 14 shows the variation of soil displacement when the cables were subjected to different prestresses. Clearly, displacement increased with increase in prestress, and the affected area also increased (Figure 15). Therefore, the deformation response increased with increase in cable prestress.

To verify the effectiveness of the proposed calculation method, in this section, the calculation results are compared with the numerical simulation results. From the results of the computational formula, Equation (34), and the numerical simulation, as shown in Figure 16, the variation of the effective depth of soil showed similar trends; the effective depth increased with increase in prestress. As shown in Figure 16, the slope of the curve in numerical simulation was relatively small when the pretension was <1000 kPa, and the effective depth increased sharply to 1500 kPa. This was attributed to the five cables working simultaneously in the numerical simulation; however, we only focused on one cable in the computational formula method. At a small value of pretension, the five cables coworked under the action of the anchor beam, and they were not fully functional. At a sufficiently large value of pretension, the cables were exploited; the effective depth of soil was determined to be slightly larger than the computational formula.

In Case 2, the variation in shear strength of soil with different anisotropy coefficients was obtained. The shear strength of soil was equal to the shear stress. Equation (16) illustrates the relationship between the cohesion of soil in the horizontal and vertical directions. Equation (17) shows the cohesive force of the saturated and undrained clay soil; c_Ψ was influenced by the anisotropy coefficient of soil. Therefore, assuming that the cables were subjected to a prestress of 500 kPa, the displacement and stress responses of the slope were obtained. Figure 17 shows that the shear strength of soil decreased with increase in the value of ρ. This is because the cohesive force of the clay, c_Ψ, decreased with increase in the value of ρ, showing an obvious influence on the strength of soil.

In Case 3, the variation in shear strength with the cohesion gradient was obtained. The strength of saturated and undrained clay soil varies linearly with depth [25–27]. According to Equation (19), when the anisotropy coefficient was 1, the cohesive force of soil increased with increase in the value of λ and the depth along the cable. As shown in Figure 18, the shear strength of soil increased with increase in the coefficient of anisotropy.

Thus, the influence of the parameters p_0, λ, and ρ was investigated successively. The response of soil underlying the cable beam was also obtained. The results of numerical simulation verified that there is good agreement with the theoretical formulas proposed in Section 3.

6. Conclusions

Based on the assumption that an anchor beam is completely rigid and a prestressed anchor cable is applied to soil in the form of uniform load, this study presents an analysis on the responses of a prestressed anchor beam, considering nonhomogeneity and anisotropy of saturated soft clay. The computational formula of superimposed stress of soil underlying the anchor beam was proposed. Plastic failure envelopes of soil and the maximum effective depth underlying the anchor beam were obtained using the D-P yield criterion, which is typically used for soft clay analysis. The validity of the proposed method was checked for agreement with the findings of previous studies. Finally, a parametric study was conducted to analyze the influence on the plastic failure envelopes and the maximum effective depth of soil underlying the anchor beam, and an intuitive numerical simulation model was established for verifying the proposed equations. Some new findings are summarized as follows:

The plastic failure envelopes of soil increased with increase in the prestress and anisotropy coefficient, and it

decreased with increase in the gradient of linear variation in cohesive force.

The maximum effective depth of soil underlying the anchor beam increased with increase in the prestress and decreased with increase in the gradient of linear variation in cohesive force. The anisotropy coefficient had a greater influence on the failure envelopes as well as on the maximum effective depth of soil at higher prestress.

The shear strength of soil decreased with increase in the anisotropy coefficient and increased with increase in the gradient of cohesive force.

Comparing the results of the computational formula and numerical simulation, there were similar variations in the effective depth of soil, that is, it increased with increase in the prestress. Because of the coworking effect of the five cables in the numerical simulation, the effective depth of soil was smaller than that calculated using the computational formula when the pretension was <1000 kPa. With increase in pretension, the cables gradually functioned, and the effective depth of soil increased sharply and was finally larger than that of the computational formula.

The proposed method and the study results can help optimize cable design parameters such as anchorage length of the cable and grouting radius.

Data Availability

All data, models, and code generated or used during the study appear in the submitted article.

Conflicts of Interest

The authors declare that there is no conflict of interest regarding the publication of this paper.

Acknowledgments

The authors gratefully acknowledge the financial support offered by the National Natural Science Foundation of China (52078311); Young Talent Top Project of Hebei Province (BJ2020055); Hebei Provincial Natural Science Foundation of China (E2019210356); Natural Science Foundation for Youths of Hebei Province of China (E2021210055); Science and Technology Research Project of Colleges and Universities in Hebei Province (Grant Number: ZD2022073); State Key Laboratory for GeoMechanics and Deep Underground Engineering, China University of Mining and Technology (SKLGDUEK1916); China Postdoctoral Science Foundation (2019M663553); Key Laboratory of Large Structure Health Monitoring and Control (KLLSHMC1903); Shenzhen Science and Technology Innovation Program (KQTD20180412181337494) and Innovation and Entrepreneurship Training Program for College Students (S202210107051).

References

[1] S. G. Du, C. Saroglou, Y. F. Chen, H. Lin, and R. Yong, "A new approach for evaluation of slope stability in large open-pit mines: a case study at the Dexing copper mine, China," *Environmental Earth Sciences*, vol. 81, no. 3, p. 102, 2022.

[2] Y. Tang, H. Lin, Y. X. Wang, and Y. L. Zhao, "Rock slope stability analysis considering the effect of locked section," *Bulletin of Engineering Geology and the Environment*, vol. 80, no. 9, pp. 7241–7251, 2021.

[3] B. X. Yuan, Z. H. Li, Z. L. Su, Q. Z. Luo, M. J. Chen, and Z. Q. Zhao, "Sensitivity of multistage fill slope based on finite element model," *Advances in Civil Engineering*, vol. 2021, Article ID 6622936, 13 pages, 2021.

[4] Y. F. Chen, H. Lin, R. H. Cao, and C. Y. Zhang, "Slope stability analysis considering different contributions of shear strength parameters," *International Journal of Geomechanics*, vol. 21, no. 3, article 04020265, 2021.

[5] L. K. Cheng, J. L. Fan, J. Han, and J. P. Xu, *Rock-Soil Anchor*, China Architecture and Building Press, Beijing, 2003.

[6] F. Delhomme, G. Debicki, and Z. Chaib, "Experimental behaviour of anchor bolts under pullout and relaxation tests," *Construction and Building Materials*, vol. 24, no. 3, pp. 266–274, 2010.

[7] F. Delhomme and G. Debicki, "Numerical modelling of anchor bolts under pullout and relaxation tests," *Construction and Building Materials*, vol. 24, no. 7, pp. 1232–1238, 2010.

[8] C. A. You and Y. B. Zhan, "Distributing law and analysis of stresses at anchoring sections of prestressed cables," *Chinese Journal of Rock Mechanics and Engineering*, vol. 24, no. 6, pp. 925–928, 2005.

[9] S. R. Wang, Y. H. Wang, J. Gong, Z. L. Wang, Q. X. Huang, and F. L. Kong, "Failure mechanism and constitutive relation for an anchorage segment of an anchor cable under pull-out loading," *Acta Mechanica*, vol. 231, no. 8, pp. 3305–3317, 2020.

[10] Q. P. Xia, J. P. Gao, L. C. Chen, and A. T. Wang, "Distribution of soil pressure on back of suspension anchor retaining wall," *Chinese Journal of Highway and Transportation Research and Development*, vol. 36, no. 7, pp. 47–52, 2019.

[11] X. Fu, J. J. Zhang, and L. R. Zhou, "Shaking table test of seismic response of slope reinforced by combination of anti-slide piles and multi-frame foundation beam with anchor cable," *Rock and Soil Mechanics*, vol. 38, no. 2, pp. 462–470, 2017.

[12] Z. P. Yang, S. Q. Li, Y. Yu, X. R. Liu, and Y. X. Hu, "Study on the variation characteristics of the anchor cable prestress based on field monitoring in a foundation pit," *Arabian Journal of Geosciences*, vol. 13, no. 23, p. 1269, 2020.

[13] J. C. Gu, Z. Q. Ming, and J. Shen, "Field testing study on load distribution of inner-anchor segment of prestress anchorage cable," *Chinese Journal of Rock Mechanics and Engineering*, vol. 17, pp. 251–256, 1998.

[14] Q. W. Xu, C. A. You, and H. H. Zhu, "Research on 3D numerieal simulation of prestressed anchor cable and its anchoring mechanism," *Chinese Journal of Underground space and Engineering*, vol. 1, no. 2, pp. 214–218, 2005.

[15] X. L. Ding, Q. Sheng, and J. Han, "Numerical simulation testing study on reinforcement mechanism of prestress anchorage cable," *Chinese Journal of Rock Mechanics and Engineering*, vol. 21, no. 7, pp. 980–988, 2002.

[16] P. Yu and Y. Yu, "Test study on prestressed anchor rope in landslide," *The Chinese Journal of Geological Hazard and Control*, vol. 7, no. 1, pp. 59–63, 1996.

[17] Z. J. Wu, Z. J. Wang, J. W. Bi, X. Fu, and Y. Yao, "Shaking table test on the seismic responses of a slope reinforced by prestressed anchor cables and double-row antisliding piles," *Shock and Vibration*, vol. 2021, Article ID 9952380, 13 pages, 2021.

[18] X. Sun, B. Zhang, L. Gan, Z. Tao, and C. Zhao, "Application of constant resistance and large deformation anchor cable in soft rock highway tunnel," *Advances in Civil Engineering*, vol. 2019, Article ID 4347302, 19 pages, 2019.

[19] Y. H. Yuan, M. Xiao, and J. T. Chen, "A method for simulating stress distribution along fully grouted anchor," *Rock and Soil Mechanics*, vol. 39, no. 5, pp. 1908–1961, 2018.

[20] M. S. Huang, H. L. Qin, and Y. C. Guo, "Upper bound solution for bearing capacity of nonhomogeneous and anisotropic clay foundation," *Chinese Journal of Rock Mechanics and Engineering*, vol. 27, no. 3, pp. 511–518, 2008.

[21] H. L. Qin, Y. J. Wang, Z. D. Tang, and S. K. Ma, "Upper bound solutions for bearing capacity of smooth rigid strip foundations on anisotropic and non-homogeneous clay," *Rock and Soil Mechanics*, vol. 32, no. 2, pp. 611–616, 2011.

[22] Y. H. Huang, "Finite Element Analysis of Nonlinear Soil Media," in *Proc. of the Symposium on Application of FEM in Civil Engineering*, pp. 663–685, New York, ASCE, 1969.

[23] S. M. He, "Modified layer-summation based on elastoplastic theory," *Rock and Soil Mechanics*, vol. 24, no. 1, pp. 81–92, 2003.

[24] X. F. Wu, G. F. Li, and J. H. Luo, "Stress formula of soil under horizontal line load," *Natural Science Journal of Hainan University*, vol. 30, no. 3, pp. 219–224, 2012.

[25] K. Y. Lo, "Stability of slopes in anisotropic soils," *Journal of the Soil Mechanics and Foundations Division*, vol. 91, no. 4, pp. 85–106, 1965.

[26] W. F. Chen, *Limit Analysis and Soil Plasticity*, Elsevier Science, The Netherlands, 1975.

[27] A. A. Al-karni and M. A. Al-shamrani, "Study of the effect of soil anisotropy on slope stability using method of slices," *Computers and Geotechnics*, vol. 26, no. 2, pp. 83–103, 2000.

[28] A. Casagrande and N. Carillo, "Shear failure of anisotropic materials," *Journal of Boston Society of Civil Engineers*, vol. 31, no. 4, pp. 74–81, 1944.

[29] S. Gourvenec and M. Randolph, "Effect of strength nonhomogeneity on the shape of failure envelopes for combined loading of strip and circular foundations on clay," *GEN*, vol. 53, no. 6, pp. 575–586, 2003.

[30] R. E. Gibson, "The analytical method in soil mechanics," *Geotechnique*, vol. 24, no. 2, pp. 115–140, 1974.

[31] A. W. Skempton, "The pore-pressure coefficient in saturated soils," *Geotechnique*, vol. 10, no. 4, pp. 186-187, 1960.

[32] P. E. Li and Y. Q. Yin, "Modification of Drucker-Prager criterion in tensile shear region," *Chinese Journal of Rock Mechanics and Engineering*, vol. 29, no. S1, pp. 3029–3033, 2010.

[33] X. H. Chu and Y. J. Xu, "Studies on transformation from M-C criterion to Drucker-Prager criterions based on distortion energy density," *Rock and Soil Mechanics*, vol. 30, no. 10, pp. 2985–2990, 2009.